AGU PUBLICATIONS

Geophysical Research Letters

RESEARCH LETTER
10.1002/2017GL075283

Key Points:
- Experimentally determined Mg partitioning between iron-rich liquid and silicate melt
- Mg partitioning depends strongly on the oxygen content in iron-rich liquid
- MgO exsolution during core cooling is drastically reduced and insufficient to drive an early geodynamo alone

Supporting Information:
- Supporting Information S1

Correspondence to:
Z. Du,
zdu@carnegiescience.edu

Citation:
Du, Z., Jackson, C., Bennett, N., Driscoll, P., Deng, J., Lee, K. K. M., … Fei, Y. (2017). Insufficient energy from MgO exsolution to power early geodynamo. *Geophysical Research Letters*, *44*. https://doi.org/10.1002/2017GL075283

Received 11 AUG 2017
Accepted 10 NOV 2017
Accepted article online 13 NOV 2017

Insufficient Energy From MgO Exsolution to Power Early Geodynamo

Zhixue Du[1], Colin Jackson[1,2], Neil Bennett[1], Peter Driscoll[3], Jie Deng[4], Kanani K. M. Lee[4], Eran Greenberg[5], Vitali B. Prakapenka[5], and Yingwei Fei[1]

[1]Geophysical Laboratory, Carnegie Institution of Washington, Washington, DC, USA, [2]National Museum of Natural History, Smithsonian Institution, Washington, DC, USA, [3]Department of Terrestrial Magnetism, Carnegie Institution of Washington, Washington, DC, USA, [4]Department of Geology and Geophysics, Yale University, New Haven, CT, USA, [5]Center for Advanced Radiation Sources, University of Chicago, Chicago, IL, USA

Abstract The origin of Earth's ancient magnetic field is an outstanding problem. It has recently been proposed that exsolution of MgO from the core may provide sufficient energy to drive an early geodynamo. Here we present new experiments on Mg partitioning between iron-rich liquids and silicate/oxide melts. Our results indicate that Mg partitioning depends strongly on the oxygen content in the iron-rich liquid, in contrast to previous findings that it depends only on temperature. Consequently, MgO exsolution during core cooling is drastically reduced and insufficient to drive an early geodynamo alone. Using the new experimental data, our thermal model predicts inner core nucleation at ~850 Ma and a nearly constant paleointensity.

1. Introduction

Paleomagnetic evidence suggests that the terrestrial magnetic field has persisted since early in Earth's history (Biggin et al., 2015; Tarduno et al., 2015). However, the energetics of the Earth and newly refined thermal conductivity values for the core (de Koker et al., 2012; Pozzo et al., 2012) appear to preclude an early dynamo. Although the thermal conductivity of the core remains controversial (Konopkova et al., 2016; Ohta et al., 2016), several mechanisms have now been proposed to resolve this "new core paradox" (Olson, 2013), including a large amount of core radioactivity (Driscoll & Bercovici, 2014) or exsolution of MgO (Badro et al., 2016; O'Rourke & Stevenson, 2016) or SiO_2 (Hirose et al., 2017). The work of the MgO exsolution model during core cooling (Badro et al., 2016; O'Rourke & Stevenson, 2016) relies on an apparent strong temperature dependence of the metal-silicate partitioning of Mg. However, controlling factors on the metal-silicate partitioning of Mg are not fully understood. Here we provide a new suite of experimental data on the partitioning of Mg between liquid iron and silicate or oxide melts that reveal crucial compositional dependence. The results show that temperature has a limited effect on MgO exsolution and therefore cannot provide necessary power alone to drive the early geodynamo.

2. Materials and Methods

Our experiments consist of metal-silicate partitioning experiments under Earth's core formation conditions using a laser-heated diamond-anvil cell. Mantle and core materials in the experiments are represented by pyrolite (or basalt, ferropericlase) and Fe (or FeSi alloy, or Fe-FeS mixture), respectively. These materials are equilibrated at temperatures and pressures of 3000–5000 K and 20–66 gigapascal (GPa). Melting is identified in situ by the appearance of a diffuse signal in X-ray diffraction patterns (Figure S1) and then confirmed ex situ from the textural appearance of recovered run products (Figure S2). Where melting has occurred, heated spot are composed of an iron-rich metallic bleb surrounded by a quenched silicate/oxide melt (Figure S2). Quenched melt spots are exposed for analysis by focused-ion-beam milling and composition characterized using a field-emission electron microprobe (FE-EMP) with a spatial resolution of ~1 μm (supporting information).

The reaction between MgO in the silicate melt and iron-rich liquid can be described as follows:

$$MgO^{silicate\ \ melt} + Fe^{metal} \rightleftharpoons FeO^{silicate\ \ melt} + Mg^{metal} \quad (1)$$

The exchange coefficient for the reaction above is defined as: $K_{Mg} = X_{FeO}X_{Mg}/(X_{Fe}X_{MgO})$, where X_{FeO} and X_{MgO} are the mole fraction of FeO and MgO component in silicate melt, respectively, while X_{Mg}, X_{Fe} are the Fe, Mg components in iron-rich liquid metal, respectively.

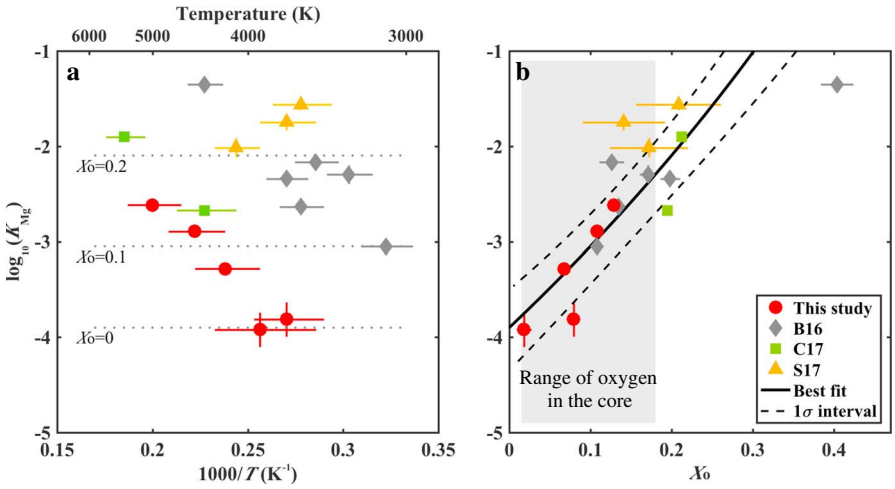

Figure 1. Exchange coefficient (K_{Mg}) as a function of (a) reciprocal temperature (1,000/T) and (b) X_O, oxygen content in iron-rich liquid metal (mole fraction) in red circles (this study), gray diamonds (B16) (Badro et al., 2016), green squares (C17) (Chidester et al., 2017), and yellow triangles (S17) (Suer et al., 2017). Experimental data for this study are shown in Extended Data Table S1. Error bars correspond to 1σ experimental uncertainties. In Figure 1a, contours of K_{Mg} at X_O = 0, 0.1, 0.2, are shown in gray dotted lines. In Figure 1b, the best fit line from weighted linear least squares fit and the 1σ confidence interval are shown in solid and dashed curves, respectively. The range of estimates for the oxygen content in the core is shown in the shaded region (e.g., Badro et al., 2015; Fischer et al., 2015; Huang et al., 2011; O'Rourke & Stevenson, 2016; Rubie et al., 2011; Wade & Wood, 2005). Also note that the experiment "16cc33C" is not plotted because Mg content in iron-rich liquid is below detection limit.

3. Data

The measured K_{Mg} values from our experiments (Table S1) are much lower at a given temperature than the previous studies of (Badro et al., 2016) and (Suer et al., 2017) but consistent with (Chidester et al., 2017) (referred to as BS16, S17, and C17, respectively) (Figure 1a). Moreover, for our results alone, we find that K_{Mg} is positively correlated with temperature, which is also the case for each individual study (Badro et al., 2016; Chidester et al., 2017; Suer et al., 2017). There are major discrepancies, however, between this study and previous studies (Badro et al., 2016; Suer et al., 2017). It is possible some of this discrepancy could be associated with uncertainties in the temperature measurement (Deng et al., 2017), but either systematic temperature overestimation (Badro et al., 2016; Suer et al., 2017) or temperature underestimation (this study; (Chidester et al., 2017)) by at least 1200 K is required to reconcile the discrepancy. On the other hand, Figure 1b reveals a strong correlation between the K_{Mg} and oxygen content in the iron-rich liquid (X_O) among all studies without invoking temperature discrepancy. This suggests that K_{Mg} must strongly depend on X_O rather than temperature alone.

4. Results

Following the previous approach (Ma, 2001) and considering the low concentration of Mg ($X_{Mg} < 0.01$), we neglect the self-interaction term and higher than first-order terms and therefore K_{Mg} can be parameterized as follows:

$$\log_{10}(K_{Mg}) = a + b/T + cP/T + d\log_{10}(1 - X_O)$$

where T is temperature in kelvin and P is pressure in GPa; X_O is the mole fraction of oxygen in the iron-rich liquid. Parameters a, b, c, and d are determined from a weighted linear least squares fit to our combined data set (supporting information). We note that the interaction parameter d is assumed to be a constant in our regression, unlike some previous studies where the interaction parameters are inversely proportional to temperature (e.g., Wade & Wood, 2005). We then regress the data set including those from this study (Table S1) and previous studies (Badro et al., 2016; Chidester et al., 2017; Suer et al., 2017). It yields:

$$\log_{10}(K_{Mg}) = -3.9(0.2) - 18.6(2)\log_{10}(1 - X_O)$$

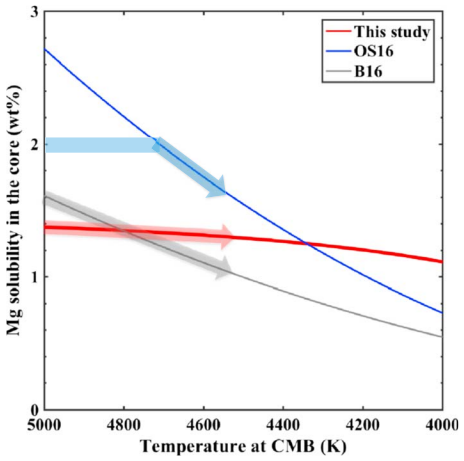

Figure 2. Calculated Mg solubility in the Earth's core as a function of temperature at CMB pressure (136 GPa), based on the K_{Mg} from this study (red) and previous studies OS16 (O'Rourke & Stevenson, 2016) (blue), while other model parameters are identical. Model results from B16 (Badro et al., 2016) are also shown in gray for comparison. Blue, gray, and red arrows show the exsolution process with initially 2 wt % Mg, 1.6 wt %, 1.4 wt % Mg in the core, for OS16, B16, and this study, respectively. Note that Badro et al. (2016) also includes an initial period of cooling before exsolution begins.

Standard errors are shown in parentheses. Parameters b and c are found to be statistically insignificant after applying an F test (P value >0.05) (supporting information). Thus, K_{Mg} is better correlated with X_O compared to $1/T$ (Figure 1), suggesting a strong role for O in stabilizing Mg in Fe alloy and a lesser role for temperature. Similar behavior was found for many other elements, in particular, V, Cr, where O greatly enhances their core partitioning (Fischer et al., 2015; Siebert et al., 2013). We note that the $1/T$ term is related with enthalpy change of reaction (1), but a $1/T$ term is not required to explain the variations of K_{Mg} among different studies. Our finding contrasts with previous studies that found (Badro et al., 2016) or assumed (O'Rourke & Stevenson, 2016) that Mg partitioning strongly depends on temperature only (Figure S3a). Instead, the discrepancies among different studies can be largely explained by the variations of X_O (Figure 1b) (Badro et al., 2016; Chidester et al., 2017; Suer et al., 2017). The overall lower X_O in this study is probably due to higher carbon contents than those in previous studies (Badro et al., 2016; Suer et al., 2017), although carbon contents were not reported. Furthermore, this might be caused by the strong interactions between carbon and oxygen in the iron-rich liquid (Fischer et al., 2015).

The strong dependence of K_{Mg} on X_O (Figure 1b) indicates Mg exsolution is intimately connected to the oxygen content of the core during cooling. Moreover, X_O likely depends on T, P, and core composition (Figure S4), consistent with previous studies on oxygen partitioning in the core (e.g., Fischer et al., 2015, and references therein). Therefore, MgO exsolution indirectly depends on T, but it is drastically reduced due to the much weaker temperature dependence of K_{Mg} than previous studies (Badro et al., 2016; O'Rourke & Stevenson, 2016). To further explore the geophysical implications, we constructed an exsolution model for the Earth's core and couple it with a thermal model of the Earth, aiming to fully understand the effect of MgO exsolution on the Earth's thermal evolution. In the end, combined with paleomagnetic records, we offer potential observational tests for exsolution and inner core nucleation (ICN).

5. Geophysical Implications

We use the exchange coefficient, K_{Mg}, to calculate Mg solubility in the core during cooling (supporting information). Because of the uncertainties of temperatures, pressures, and core compositions in the core formation processes (Badro et al., 2016; O'Rourke & Stevenson, 2016), we treat the initial Mg content of the core as a free parameter and it ranges between 0 and 2 wt %. We adopt the model from O'Rourke and Stevenson (2016) for exsolution of an MgO-rich component: after Earth's core formation, initial concentrations of 0–2 wt % Mg, 3 wt % Si, and 6 wt % O are assumed to be well mixed and homogeneously dissolved in the core (O'Rourke & Stevenson, 2016). As the core cools, exsolution occurs within the core near the core mantle boundary (CMB) where the buoyant MgO-rich exsolution is instantaneously removed from the core.

Calculated Mg solubility in the core, assuming exsolution as a liquid, is shown in Figure 2, using K_{Mg} from this study and O'Rourke and Stevenson (2016), while keeping all other model parameters identical. Model results from Badro et al. (2016) are also shown as gray curve for comparisons (Figure 2). Calculated results (Figure 2) show a very weak temperature dependence of Mg solubility (change of Mg solubility ~0.3 wt % from 5000 K to 4000 K), much weaker than previous studies, for example, 1 wt % (Badro et al., 2016) and 3 wt % (O'Rourke & Stevenson, 2016). Importantly, this implies very limited exsolution of MgO out of the core during cooling. We also predict an MgO-rich exsolution, similar to previous studies (O'Rourke & Stevenson, 2016) in the range of 4000–5000 K (Figure S5).

To illustrate the exsolution process, we consider initially 1.4 wt % Mg (Figure 2). As the core cools, Mg content follows the red solid curve to the present-day value of ~1.1 wt %. In comparison, for results from OS16 (O'Rourke & Stevenson, 2016) with an initial 2 wt % Mg, the core is undersaturated in Mg; therefore,

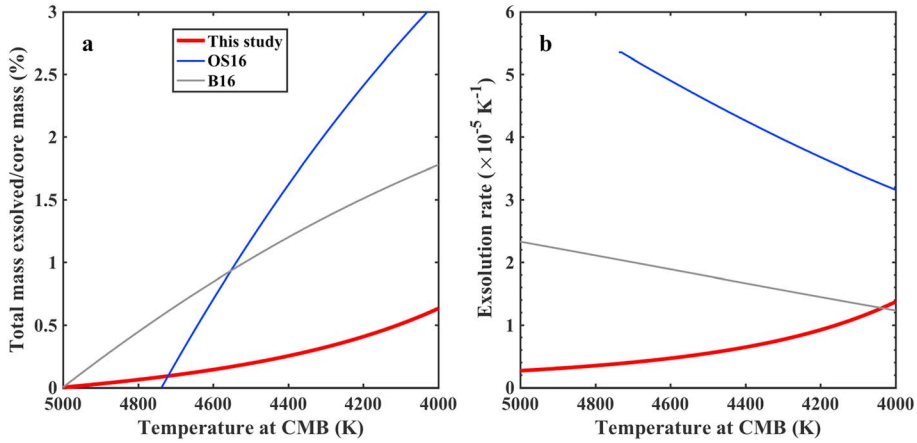

Figure 3. Calculated (a) total mass exsolved normalized to core mass and (b) exsolution rate as function of temperature at CMB pressure. Results assuming K_{Mg} from this study (red) and that from OS16 (O'Rourke & Stevenson, 2016) (blue) are shown, with other model parameters identical. Model results from B16 (Badro et al., 2016) are also shown in gray. For simplicity, inner core formation is not considered in this calculation but its effect is shown in Figure 4.

exsolution does not occur until ~4750 K. Subsequently, the Mg content drops along the blue dashed curve to ~0.7 wt % due to the strong temperature dependence. Similarly, the model results from B16 (Badro et al., 2016) are shown in the gray curve. This estimate of core Mg content at present day of ~1.1 wt % is an upper limit and could be further constrained by density and sound speed effects.

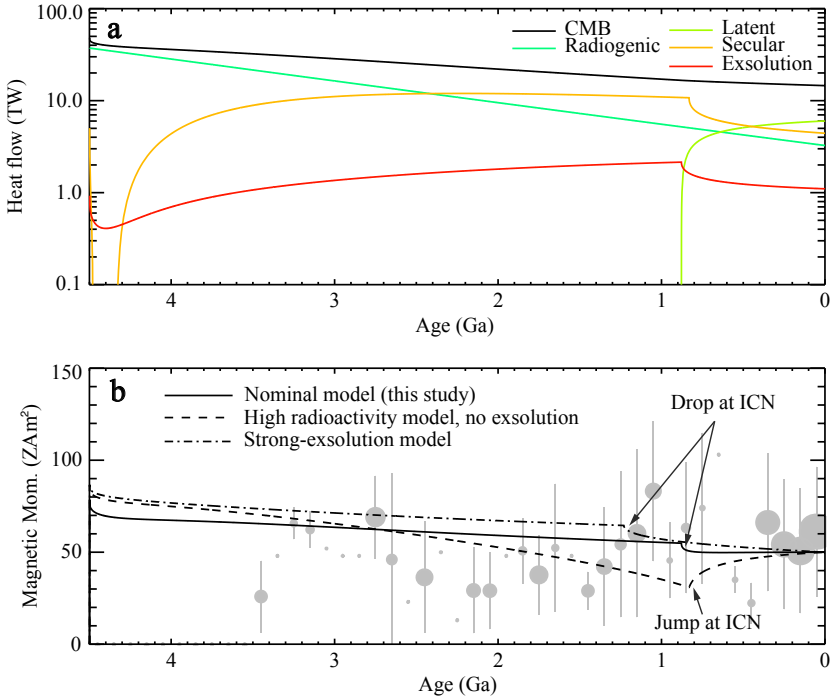

Figure 4. (a) Core heat flows in the "nominal" model with exsolution determined by this study and 3.2 TW of core radioactivity. (b) Rescaled magnetic moment throughout Earth's history for three models: (1) a "nominal" model with exsolution determined by this study and 3.2 TW of core radioactivity (black), (2) a "high radioactivity" model without exsolution but with 3.7 TW of core radioactivity (dashed), and (3) a strong-exsolution model with 9 times greater exsolution energy than this study and no core radioactivity (dash-dotted line). Virtual dipole moment (VDM) paleointensity data are from the Absolute Paleointensity (PINT) Database in Biggin et al. (2009) (circles). VDM data are the average within 100 Myr long bins with symbol size in logarithmic proportion to the number of data in each bin, error bars denote standard deviation of average within each bin, and bins with a single data point are shown as dots without error bars. More details on the nominal model are shown in Figure S6.

Following each Mg solubility curve in Figure 2, we calculate the total mass exsolved and exsolution rate as a function of temperature at CMB pressure (Figure 3). Our partitioning behavior produces a much lower exsolution rate than previously proposed (2×10^{-5} K^{-1}) (O'Rourke et al., 2017) to drive an early geodynamo (Figure 3b). We also note that exsolution rate increases as temperature decreases for this study in contrast to previous studies (Badro et al., 2016; O'Rourke & Stevenson, 2016), which is primarily due to the strong dependence of K_{Mg} on X_O. As the temperature decreases, X_O decreases and this in turn increases the exsolution rate.

To demonstrate the effect of exsolution on the thermal history of the core and the early geodynamo, we couple our predicted total (gravitation and reaction) MgO exsolution energy with a thermal model of the core (Driscoll & Bercovici, 2014) (supporting information). We compute three models (Figure 4b): (1) a "nominal" model with our experimental partitioning and 3.2 TW of core radioactivity (~400 ppm), as required to produce the present IC (inner core) size; (2) a "high radioactivity" model where no exsolution occurs, and 3.7 TW of core radioactivity is required; and (3) a "strong-exsolution" model with an exsolution rate 9 times the rate of the nominal model and no core radioactivity is needed. This latter model is similar to previous studies with strong exsolution either as MgO (Badro et al., 2016; O'Rourke & Stevenson, 2016) or SiO_2 (Hirose et al., 2017).

We note that such a large radioactive heat source (≥3.2 TW) is not favored for the core (e.g., Chidester et al., 2017; Corgne et al., 2007; Hirao et al., 2006) but is often assumed in order to match the empirical constraints (surface heat flow of 39 TW, upper mantle temperature of 1630 K, inner core radius 1221 km, and continuous dynamo) (e.g., Driscoll & Bercovici, 2014; Nimmo et al., 2004). To compare with paleomagnetic data (Biggin et al., 2015), we rescale the magnetic moment predicted by our models assuming present-day value ~50 ZAm^2 (Figure 4b).

The nominal model produces ~1 TW from exsolution (Figure 4a), which powers the dynamo but still requires unreasonably high radioactivity. The nominal model also predicts an IC age of ~850 Ma and a nearly constant magnetic moment history similar to the strong-exsolution model (Figure 4b) (O'Rourke et al., 2017). This is because in both cases exsolution dominates the buoyancy throughout Earth's history due to its high efficiency in generating buoyancy flux. Interestingly, both exsolution models produce drops in the magnetic moment following ICN (Figure 4b). These drops in magnetic moment are caused by a rapid decrease in the core secular cooling rate at ICN due to latent heat release at the ICB, which then results in a drop in exsolution rate and magnetic moment.

This is in contrast to a jump after ICN for the high radioactivity models (no exsolution) where compositional buoyancy driven by IC solidification dominates (Driscoll, 2016; Driscoll & Bercovici, 2014). Therefore, a drop in magnetic moment at ICN may offer an observational test for the exsolution. Additional high quality paleomagnetic data around 0.5–1 Ga would help to test this hypothesis (Biggin et al., 2009; Driscoll, 2016).

6. Conclusions

Based on our new interpretation of the Mg partitioning data, powering the early geodynamo requires a substantial alternative heat source. High core radioactivity would provide such a heat source but is unrealistic on the geochemical grounds (e.g., Chidester et al., 2017; Corgne et al., 2007; Hirao et al., 2006). The strong-exsolution model works if the core cooling rate is strongly coupled to its compositional evolution, particularly the change of oxygen content in the core. It has been suggested that oxygen in the core might be exhausted by SiO_2 exsolution (Hirose et al., 2017), and thus, MgO and SiO_2 exsolution may be coupled. In summary, we find that that MgO exsolution is unlikely to provide the power needed to drive the early geodynamo.

Acknowledgments

Data supporting Figure S1 are available in supporting information Table S1. We thank Emma Bullock for electron microprobe analysis, Suzy Vitale for FIB operations, and Victor Lugo for machining at Carnegie Institution of Washington. We also thank Sz-Chian Liou at University of Maryland and Fernando Camino at Brookhaven National Lab for help with FIB operations. We thank Timothy Strobel and Alexander Goncharov's generosity for sharing laser systems and other facilities. Special thanks for Jiachao Liu and Jie Li for donating a carbon standard and Stephen Elardo for synthesizing the basalt glass. We also thank Anat Shahar, Miki Nakajima, Renbiao Tao, Megan Duncan, and James Badro for discussions. We appreciate two anonymous reviewers for critical comments. Z. Du, C. Jackson, and N. Bennett thank the Carnegie Fellowship for financial support. The research is supported by NSF grant (EAR-1447311) to Y. Fei. Work at Yale University is supported in part by NSF grants (EAR-1321956 and EAR-1551348) to K. K. M. Lee. Portions of this work were performed at GeoSoilEnviroCARS (University of Chicago, Sector 13), Advanced Photon Source (APS), Argonne National Laboratory. GeoSoilEnviroCARS is supported by the National Science Foundation-Earth Sciences (EAR-1128799) and Department of Energy-GeoSciences (DE-FG02-94ER14466). This research used resources of the Advanced Photon Source, a U.S. Department of Energy (DOE) Office of Science User Facility operated for the DOE Office of Science by Argonne National Laboratory under contract DE-AC02-06CH11357.

References

Badro, J., Brodholt, P., Piet, H., Siebert, J., & Ryerson, F. J. (2015). Core formation and core composition from coupled geochemical and geophysical constraints. *Proceedings of the National Academy of Sciences of the United States of America*, *112*(40), 12,310–12,314. https://doi.org/10.1073/pnas.1505672112

Badro, J., Siebert, J., & Nimmo, F. (2016). An early geodynamo driven by exsolution of mantle components from Earth's core. *Nature*, *536*(7616), 326–328. https://doi.org/10.1038/nature18594

Biggin, A. J., Piispa, E. J., Pesonen, L. J., Holme, R., Paterson, G. A., Veikkolainen, T., & Tauxe, L. (2015). Palaeomagnetic field intensity variations suggest Mesoproterozoic inner-core nucleation. *Nature*, *526*(7572), 245–248. https://doi.org/10.1038/nature15523

Biggin, A. J., Strik, G., & Langereis, C. G. (2009). The intensity of the geomagnetic field in the late-Archaean: New measurements and an analysis of the updated IAGA palaeointensity database. *Earth, Planets and Space*, *61*(1), 9–22. https://doi.org/10.1186/BF03352881

Chidester, B. A., Rahman, Z., Righter, K., & Campbell, A. J. (2017). Metal-silicate partitioning of U: Implications for the heat budget of the core and evidence for reduced U in the mantle. *Geochimica et Cosmochimica Acta*, *199*, 1–12. https://doi.org/10.1016/j.gca.2016.11.035

Corgne, A., Keshav, S., Fei, Y., & McDonough, W. F. (2007). How much potassium is in the Earth's core? New insights from partitioning experiments. *Earth and Planetary Science Letters*, *256*(3-4), 567–576. https://doi.org/10.1016/j.epsl.2007.02.012

de Koker, N., Steinle-Neumann, G., & Vlcek, V. (2012). Electrical resistivity and thermal conductivity of liquid Fe alloys at high *P* and *T*, and heat flux in Earth's core. *Proceedings of the National Academy of Sciences of the United States of America*, *109*(11), 4070–4073. https://doi.org/10.1073/pnas.1111841109

Deng, J., Du, Z., Benedetti, L. R., & Lee, K. K. M. (2017). The influence of wavelength-dependent absorption and temperature gradients on temperature determination in laser-heated diamond-anvil cells. *Journal of Applied Physics*, *121*(2), 11.

Driscoll, P. E. (2016). Simulating 2 Ga of geodynamo history. *Geophysical Research Letters*, *43*, 5680–5687. https://doi.org/10.1002/2016GL068858

Driscoll, P. E., & Bercovici, D. (2014). On the thermal and magnetic histories of earth and Venus: Influences of melting, radioactivity, and conductivity. *Physics of the Earth and Planetary Interiors*, *236*, 36–51.

Fischer, R. A., Nakajima, Y., Campbell, A. J., Frost, D. J., Harries, D., Langenhorst, F., … Rubie, D. C. (2015). High pressure metal-silicate partitioning of Ni, Co, V, Cr, Si, and O. *Geochimica et Cosmochimica Acta*, *167*, 177–194. https://doi.org/10.1016/j.gca.2015.06.026

Hirao, N., Ohtani, E., Kondo, T., Endo, N., Kuba, T., Suzuki, T., & Kikegawa, T. (2006). Partitioning of potassium between iron and silicate at the core-mantle boundary. *Geophysical Research Letters*, *33*, L08303. https://doi.org/10.1029/2005GL025324

Hirose, K., Morard, G., Sinmyo, R., Umemoto, K., Hernlund, J., Helffrich, G., & Labrosse, S. (2017). Crystallization of silicon dioxide and compositional evolution of the Earth's core. *Nature*, *543*(7643), 99–102. https://doi.org/10.1038/nature21367

Huang, H., Fei, Y., Cai, L., Jing, F., Hu, X., Xie, H., … Gong, Z. (2011). Evidence for an oxygen-depleted liquid outer core of the Earth. *Nature*, *479*(7374), 513–516. https://doi.org/10.1038/nature10621

Konopkova, Z., McWilliams, R. S., Gomez-Perez, N., & Goncharov, A. F. (2016). Direct measurement of thermal conductivity in solid iron at planetary core conditions. *Nature*, *534*(7605), 99–101. https://doi.org/10.1038/nature18009

Ma, Z. (2001). Thermodynamic description for concentrated metallic solutions using interaction parameters. *Proceedings of Science Metallurgical and Materials Transactions B-Proceedings of Metallurgical Materials*, *32*(1), 87–103.

Nimmo, F., Price, G. D., Brodholt, J., & Gubbins, D. (2004). The influence of potassium on core and geodynamo evolution. *Geophysical Journal International*, *156*(2), 363–376. https://doi.org/10.1111/j.1365-246X.2003.02157.x

Ohta, K., Kuwayama, Y., Hirose, K., Shimizu, K., & Ohishi, Y. (2016). Experimental determination of the electrical resistivity of iron at Earth's core conditions. *Nature*, *534*(7605), 95–98. https://doi.org/10.1038/nature17957

Olson, P. (2013). The new core paradox. *Science*, *342*(6157), 431–432. https://doi.org/10.1126/science.1243477

O'Rourke, J. G., Korenaga, J., & Stevenson, D. J. (2017). Thermal evolution of Earth with magnesium precipitation in the core. *Earth and Planetary Science Letters*, *458*, 263–272. https://doi.org/10.1016/j.epsl.2016.10.057

O'Rourke, J. G., & Stevenson, D. J. (2016). Powering Earth's dynamo with magnesium precipitation from the core. *Nature*, *529*(7586), 387–389. https://doi.org/10.1038/nature16495

Pozzo, M., Davies, C., Gubbins, D., & Alfe, D. (2012). Thermal and electrical conductivity of iron at Earth's core conditions. *Nature*, *485*(7398), 355–358. https://doi.org/10.1038/nature11031

Rubie, D. C., Frost, D. J., Mann, U., Asahara, Y., Nimmo, F., Tsuno, K., … Palme, H. (2011). Heterogeneous accretion, composition and core-mantle differentiation of the Earth. *Earth and Planetary Science Letters*, *301*(1-2), 31–42. https://doi.org/10.1016/j.epsl.2010.11.030

Siebert, J., Badro, J., Antonangeli, D., & Ryerson, F. J. (2013). Terrestrial accretion under oxidizing conditions. *Science*, *339*(6124), 1194–1197. https://doi.org/10.1126/science.1227923

Suer, T.-A., Siebert, J., Remusat, L., Menguy, N., & Fiquet, G. (2017). A sulfur-poor terrestrial core inferred from metal–silicate partitioning experiments. *Earth and Planetary Science Letters*, *469*, 84–97. https://doi.org/10.1016/j.epsl.2017.04.016

Tarduno, J. A., Cottrell, R. D., Davis, W. J., Nimmo, F., & Bono, R. K. (2015). A Hadean to Paleoarchean geodynamo recorded by single zircon crystals. *Science*, *349*(6247), 521–524. https://doi.org/10.1126/science.aaa9114

Wade, J., & Wood, B. J. (2005). Core formation and the oxidation state of the Earth. *Earth and Planetary Science Letters*, *236*(1-2), 78–95. https://doi.org/10.1016/j.epsl.2005.05.017